Gold nanoparticles as absolute nano-thermometers

Aquiles Carattino, Martín Caldarola, and Michel Orrit*

Huygens-Kamerlingh Onnes Lab, 2300RA Leiden, The Netherlands

E-mail: orrit@physics.leidenuniv.nl

Anti-Stokes emission form gold nanorods

We model the photoluminescence generation in gold nanorods with successive steps taking place between absorption of light and re-emission of luminescence.[1] Figure S1 shows the energy-momentum representation of the photoluminescence processes in gold nanorods. After excitation with monocrhomatic light of energy $\hbar\omega_L$, a collective oscillation of electrons is generated, i.e. a surface plasmon (SPR). Once the coherence is lost (dephsasing time $\sim$fs), the state can be described as an electron-hole pair. Then, three scenarios are possible: electron and hole may recombine radiatively after one or more interactions with the thermal baths of lattice phonons and charge carrier thermal excitations: i) if the energy difference between electron and hole states is lower than the initial one after excitation we obtain Stokes emission upon a radiative recombination; ii) if electron and hole transiently increase their energy difference at the bath's expense before recombining radiatively, we observe anti-Stokes emission; iii) if electron and hole recombine non radiatively, their energy difference is transferred to the baths and no photon is emitted. The latter process is the most probable one, explaining the low yields of luminescence in gold.

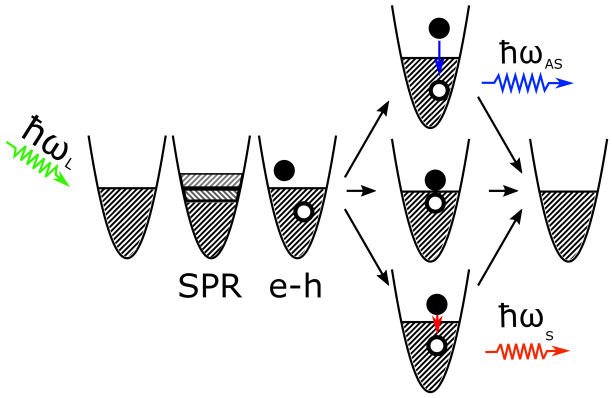

Figure S1: Anti-Stokes luminescence process from a single gold nanorod.

Experimental setup

The experimental setup consisted on a home-made confocal microscope, schematically shown in figure S2, similar to the one presented before.[1] The microscope allows the detection of individual nanorods in the sample and the measurement of their photoluminescence spectra. We use continuous wave lasers at 532 nm or 633 nm to excite the transverse and longitudinal plasmon resonances, respectively. The 532 nm is a DPSS laser (CNI) and the 633 nm is a HeNe (Thorlabs). Both lasers are reflected at a 50/50 beam splitter that allows the simultaneous detection of the anti-Stokes and Stokes emission of the particles. We employ an objective lens to focus the excitation beam into a diffraction limited spot and we collect the emitted photoluminescence using the same objective in an epi-configuration. The 532 nm laser is focused down by our 60x NA1.4 objective to a waist of 228 nm, with a power of 200μW reaching the sample, leading to an intensity of 1.23 mWμm^{-2}. For the HeNe laser, the maximum power used was 100 μW which corresponds to 0.43 mWμm^{-2}. This is equivalent to 1.37×10^{15} photons s^{-1} μm^{-2}, which leads to a fluence of ≈ 82 photonsμm^{-2} in one minute integration time used for the spectra acquisition. A confocal pinhole of 50 μm is placed between a pair of lenses with 10 cm focal length to reduce the unwanted background from the solvent above the nanorods. Then we could select between an APD or the spectrometer to perform a raster-scan image or an emission spectrum, respectively. We reject the laser light with appropriate notch filters.

Additionally, the temperature of the sample can be controlled with a special holder that allows water flow, a heater and a thermocouple to measure the temperature of the sample.

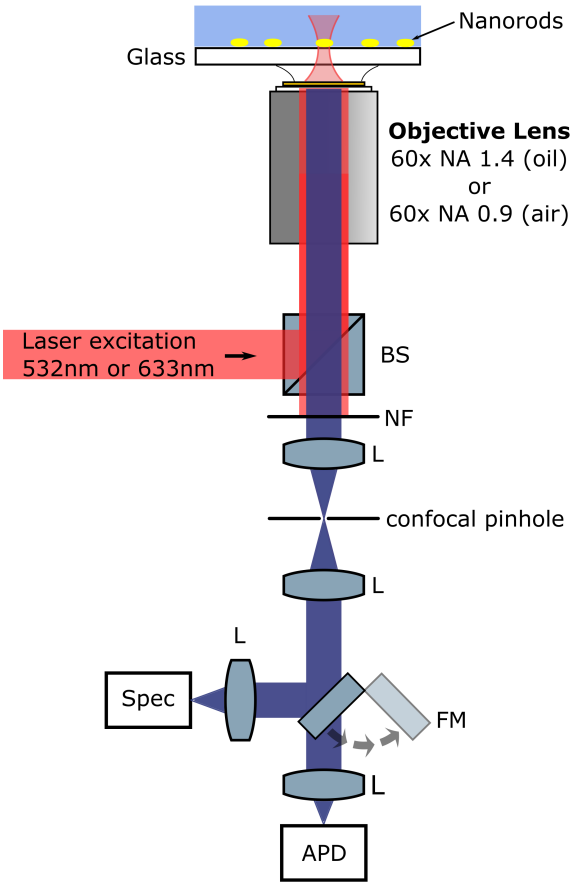

Figure S2: Scheme of the experimental setup. The sample consists of individual gold nanorods immobilized on glass. BS: beam splitter. NF: notch filter to remove excitation light and detect Stokes and anti-Stokes photoluminescence. L: lens. FM: flip mirror. SPEC: spectrometer. APD: avalanche photodiode.

Gold nanorod sample characterization

We synthesized gold nanorods using the seed-mediate grwoth method[2] and characterized their size by performing TEM imaging on a dropped cast sample on a silicon substrate. Figure S3 (a) shows the image where the cilindrical with sperical cups shape can be seen

and the width is 23 nm while the length is 50 nm, leading to a mean aspect ratio of 2.17. Naturally, there is some dispersion in the size due to the fabrication procedure, that leads to a broad bulk extinction spectra, shown in (b). The transverse plasmon resonance is located at 525 nm while the more intense longitudinal plasmon resonance is at 630 nm. We also show the wavelegnths of the lasers used for our study as vertical lines.

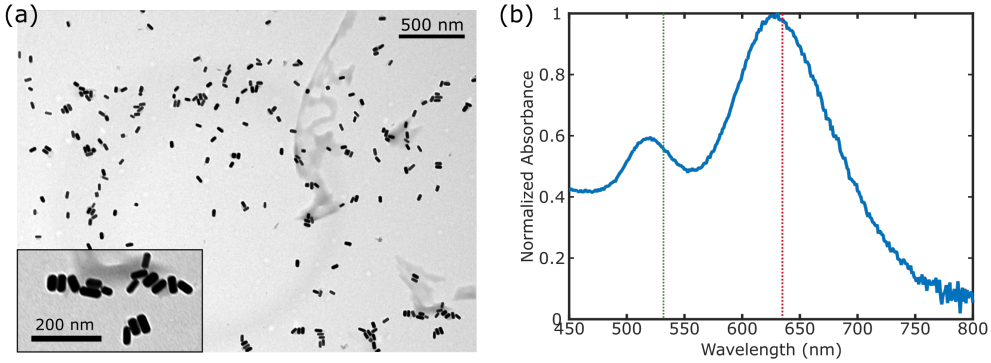

Figure S3: **Gold nanorod characterization** (a) TEM image of a dried drop of the gold nanorods used in this study. The mean width is 23 nm while the length is 50. The inset shows higher magnification. (b) Bulk absorbance spectra of the gold nanorod sample showing the transverse (around 525 nm) and the longitudinal surface (around 630 nm) plasmon resonances. The dashed vertical lines show the two laser wavelengths used in this work.

Determination of the error in the temperature extraction

The temperature extracted from the anti-Stokes spectrum depends on the initial fit of the plasmon resonance. The luminescence spectrum acquired with the 532 nm laser, shows an asymmetric shape due to a broadband contribution from gold added to the plasmonic emission. Therefore, the fitting of the SPR function ($I_{\mathrm{SPR}}(E)$) of equation 2 is not univocally determined; it will depend on the range of wavelengths selected for the fit. Therefore, the error of the method for temperature extraction can be estimated by studying the dependency of the final value with the intermediate parameters (i.e. the parameters of the lorentizan fit).

For the particle shown in Fig. 1, changing the initial wavelength of the fit from 600 nm to

640 nm yields a significative difference in the obtained parameters of the lorentzian. Using the following expression for the I_{SPR} function in eV,

$$I_{\mathrm{SPR}}(E) = \frac{P_1}{(E - P_2)^2 + P_3}$$

We find that the values of P_2 lie between 1.940 eV and 1.955 eV and P_3 values between $8 \cdot 10^{-3}$ eV^2 and $8 \cdot 10^{-3}$ eV^2 for the different wavelength ranges. The value of P_1 is not relevant for the analyzis because it is only a normalization factor.

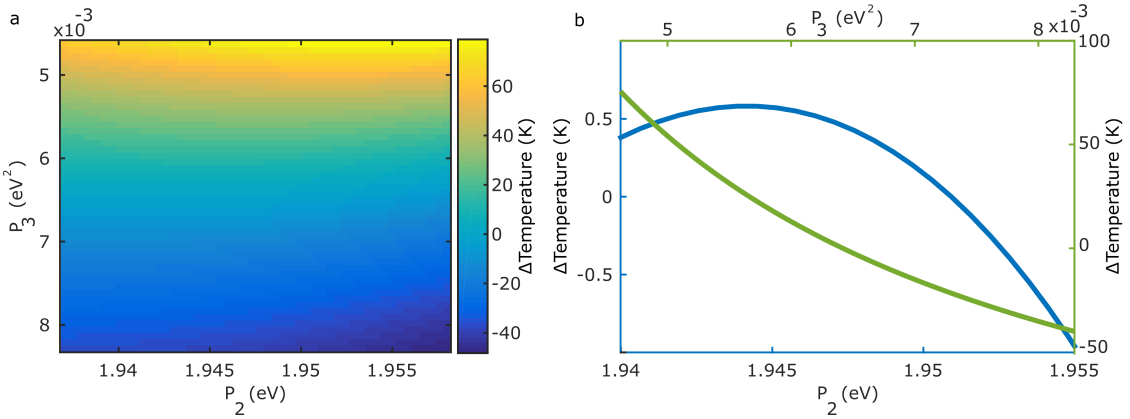

Figure S4: Estimation of the error due to different fitting parameters of the plasmon spectrum. a) 2D grid of the difference in temperature obtained while varying both P_2 and P_3 parameters of the fit. b) Temperature dependence while keeping either P_2 or P_3 constant.

To study the impact that these different parameters have on the final result, we calculate the extracted temperature for all the combinations of P_2 and P_3, as is shown in Figure S4.a. The color scale encodes the difference in temperature extracted compared to the value obtained with the parameters at the center of the range. Figure S4.b shows two cross cuts of the temperature, while keeping either P_2 or P_3 constant.

In this example it is possible to note that the measured temperature is highly dependent on the fitted width of the plasmon spectrum (P_3) but barely dependent on its peak position (P_2). From the spectrum of the particle, it is possible to note that the wing of the plasmon coincides with the range of the anti-Stokes emission. Therefore, minute changes in the shape of the resonance will yield higher changes in the extracted temperature.

This assertion also implies that there should be particles in which the extracted temperature through the anti-Stokes fit wouldn't be too sensitive to the initial plasmon fit. To explore these possibilities, we calculated the anti-Stokes emission of different particles at 400 K by using equation 2 and the results of ADDA calculations for the SPR function. From these data, we extracted the temperature while varying the lorentzian parameters, exactly in the same way as what was done for the experimental results. We can therefore study the error in temperature for particles with different plasmonic resonances.

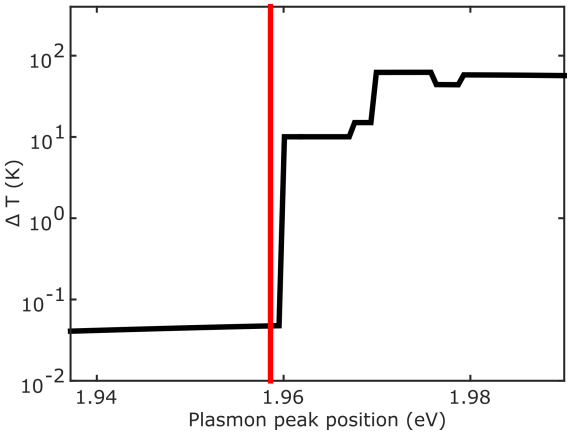

Figure S5: Calculated error in the temperature extraction due to the uncertainty in the plasmon parameters as a function of the resonance position of the particle. Clearly, when exciting at the blue wing of the plasmon, the effect of these uncertainties is much lower.

Figure S5 shows the uncertainty in the extracted temperature as a function of the plasmon peak position. The uncertainty is defined as the difference between the maximum and the minimum extracted temperatures while varying P_2 by 10% and P_3 by 30%. The vertical red line depicts the wavelength of the laser. It is remarkable that particles with a resonance red-shifted from the excitation laser present a much lower uncertanty in temperature as compared to particles with a resonance to the blue of the laser.

When the plasmon favors the anti-Stokes emission the correct modelling of the resonance is crucial for the extraction of temperatures. On the other hand, when the plasmon is red-shifted from the excitation, the induced error in the extracted temperature is much lower. However, the amount of collected light is another factor to keep into account. When the

resonance is red-shifted from the laser, the anti-Stokes emission is much weaker and therefore accumulating enough photons in the spectrometer requires longer acquisition times.

Luminescence power dependence

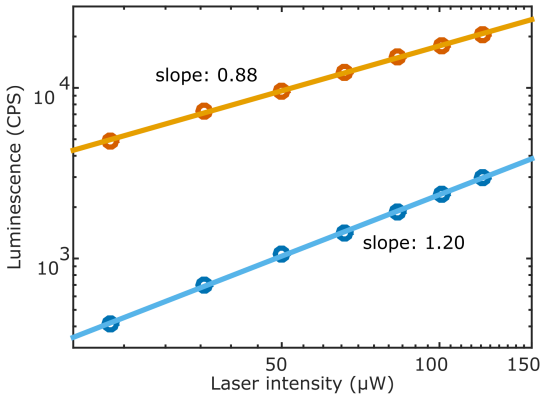

Figure S6: Stokes and anti-Stokes integrated emission as a function of excitation power. The linear fit in logarithmic scale has a slope of 0.88 and 1.20 respectively, confirming the 1-photon nature of both kinds of emission.

Figure S6 shows the intensity of the Stokes (red) and anti-Stokes (blue) emission for several excitation powers. In both cases the linear fit in logarithmic scale has a slope close to 1, being 0.88 for the Stokes and 1.20 for the anti-Stokes, confirming that both types of emission are single-photon processes. The anti-Stokes has a higher slope due to dependence on T of the anti-Stokes emission: the higher the power, the higher the temperature of the particle and the higher the anti-Stokes signal is. This behavior is independent of the plasmon resonance position. It is important to note that the excitation intensity cannot be increased much beyond what is shown because nanorods would start reshaping towards more spherical shapes at higher laser powers.

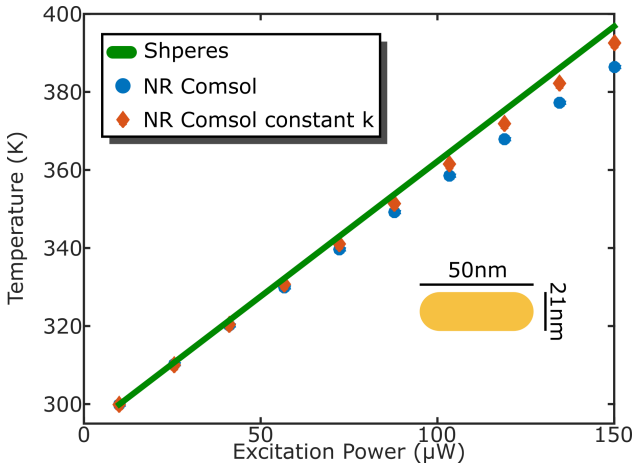

Figure S7: Calculated temperature for a nanosphere (full line) and for a 21 nm × 50 nm nanorod (dots) under different excitation intensities. The dots are numerically calculated values using COMSOL Multiphysics commercial software. The circles where obtained with the temperature-dependent heat conductivity of water and the diamonds with a constant value of $0.61\,\mathrm{W}(\mathrm{m}\cdot\mathrm{K})^{-1}$.

Gold Nanorod temperature calculations

Throughout the main text the temperature measured with the anti-Stokes emission is compared to the calculated temperature using the heat diffusion equation. For spheres in an homogeneous water environment and assuming an infinite thermal conductivity for the metal, the temperature increase is given by

$$\Delta\mathrm{T}(P) = \frac{P}{4\pi k_{\mathrm{water}} R} \tag{1}$$

where P is the dissipated power, k_{water} is the heat conductivity of water and R is the radius of the particle.[3] The dissipated power can be easily derived from the cross section of the particle at a given wavelength and the intensity of the focused laser beam. For nanorods we assumed an equivalent sphere with radius such that the total rod area is preserved.

Figure S7 shows the difference between the results from the sphere (full line) and a finite element method calculation (dots) for a nanorod of length 50 nm and diameter 21 nm. The cross section and dissipated power were kept the same. The blue circles are the results given by using the built-in material properties of water, i.e. a thermal conductivity that depends

on temperature. The diamonds are the results when the thermal conductivity is fixed to $0.61\,\mathrm{W}(\mathrm{m}\cdot\mathrm{K})^{-1}$. The difference is accentuated at higher temperatures.

References

(1) Carattino, A.; Keizer, V. I.; Schaaf, M. J.; Orrit, M. Background suppression in imaging gold nanorods through detection of anti-stokes emission. *Biophysical journal* **2016**, *111*, 2492–2499.

(2) Nikoobakht, B.; El-Sayed, M. A. Preparation and growth mechanism of gold nanorods (NRs) using seed-mediated growth method. *Chem. Mater* **2003**, *15*, 1957–1962.

(3) Baffou, G.; Quidant, R. Thermo-plasmonics: using metallic nanostructures as nano-sources of heat. *Laser Photon. Rev.* **2013**, *7*, 171–187.